Available online at www.sciencedirect.com
SCIENCE DIRECT®
Journal of Sound and Vibration 292 (2006) 802–823
JOURNAL OF SOUND AND VIBRATION
www.elsevier.com/locate/jsvi

A reciprocal band-limited Green's function approach for modelling acoustic emission using the finite element method

R.R. Naber[a,*], H. Bahai[a], B.E. Jones[b]

[a]*School of Engineering and Design, Brunel University, UB8 3PH, UK*
[b]*The Brunel Centre for Manufacturing Metrology, Brunel University, UB8 3PH, UK*

Received 21 April 2005; received in revised form 9 June 2005; accepted 5 September 2005
Available online 14 November 2005

Abstract

The ability to model acoustic emission (AE) plays an important role in advancing the reliability of AE source characterisation. In this paper, an efficient numerical approach is proposed for modelling AE waves in isotropic solids. The approach is based on evaluating the reciprocal band-limited Green's functions using the finite element (FE) method. In the first section, known analytical solutions of the Green's function for an elastic isotropic infinite plate subjected to point monopole surface loading are used to validate the approach. Then, a study investigating the effects of the spatial resolution of the FE model on the accuracy of the numerical solutions is presented. Furthermore, comparisons between numerical calculations and experimental measurements are presented for a glass plate subjected to two known AE sources (pencil lead break and ball impact). Finally, the reciprocal relation between the source and the receiver is confirmed using numerical simulations of a plane stress model of an elastic isotropic plate.

1. Introduction

Acoustic emission (AE) is defined as the transient elastic waves that are generated due to the sudden release of strain energy within materials. AE sources include cracks, dislocations, phase transformations, friction, etc. These waves give rise to small surface displacements that can be detected using piezoelectric sensors. Ideally, a technique is required that would extract from the measured AE signals accurate information about the AE sources. This information can then be used for monitoring the integrity of structures or the conditions of machines/processes.

To date, most AE monitoring systems are based on empirical analysis whereby the cause (AE source) and the effect (measured AE signals) are only inferred from a database built on numerous AE tests. Examples of this approach can be found in Ref. [1]. The difficulty with this empirical AE approach is that the correlations established between the AE source and the measured AE signals often lack general validity; they are sensitive to the parameters of the AE measurement conditions (i.e. structural geometry, material properties, type of

*Corresponding author. Tel.: +44 (0) 1895 265881; fax: +44 (0) 1895 269763.
E-mail addresses: ramez-robert.naber@brunel.ac.uk (R.R. Naber), hamid.bahai@brunel.ac.uk (H. Bahai), barry.jones@brunel.ac.uk (B.E. Jones).

0022-460X/$ - see front matter © 2005 Elsevier Ltd. All rights reserved.
doi:10.1016/j.jsv.2005.09.003

sensor, source/sensor locations, etc.). In addition, few AE measurements are often confirmed by direct observations of the AE sources due to the limitations in controlling the sources experimentally and sometimes other physical restrictions. As a result, the overall reliability of the developed AE monitoring system for AE source characterisation suffers. Nonetheless, if the AE waves can be simulated using the fundamental theoretical principles behind the generation, propagation and detection of AE, then the AE responses for known AE sources at known locations can be predicted. This would allow the development of more reliable AE monitoring systems and at lower costs which can be employed in critical engineering applications.

In this paper, an approach is proposed for modelling AE wave propagation. The approach is based on evaluating the reciprocal band-limited Green's functions of a body using the finite element (FE) method. The advantage of the proposed approach is that the technique is general and can be applied to model geometries and material properties that cannot be treated directly using closed-form analytical solutions. The approach is also efficient in the sense that it allows the results of only one FE simulation to be used for predicting the AE responses at one receiver location due to any body force (i.e. any AE source) from any location within the discretised space of the FE model. This is possible using the reciprocal relationship between the source and the receiver. The theory behind the proposed approach is explained in detail in the next section of this paper and references can be found therein.

The organisation of this paper is now outlined. Initially a validation of the FE method is presented using the known exact analytical solutions of the Green's function for an axi-symmetric model of an elastic isotropic plate with infinite lateral dimensions. Then the effect of varying the spatial resolution of FE model on the accuracy of the numerical solutions is investigated. Results are also provided comparing AE measurements taken using a high-fidelity AE sensor with predicted AE responses calculated using the proposed approach for a circular glass plate subjected to two known artificial point-like AE sources (pencil lead break and ball impact). Finally, the reciprocal relationship between the source and the receiver is confirmed using numerical solutions for a plane stress model of an elastic isotropic plate.

2. Theoretical background

2.1. Quantitative AE

Fig. 1 shows a schematic diagram of an AE measurement chain. This is the basic model used to predict AE signals in a quantitative AE analysis. The AE source is modelled using 'equivalent' body forces. These forces when applied to a body generate an identical wave field to that of the real source [2]. If the equivalent body forces for a given AE source are known, then the time-dependent displacement response at the location of the sensor can be calculated using an appropriate model of wave propagation for the structure of interest. The effects of the sensor and the detection electronics can be modelled using a transfer function, which provides the relationship between the mechanical surface displacements input and the recorded electrical voltage output at all frequencies. This transfer function can be determined from an absolute system calibration [3]. The most difficult part of the analysis is in modelling the AE wave propagation.

2.2. The Green's function method

Elastic wave propagation in solids is a vast subject that has been studied using numerous analytical, numerical and experimental methods. A review of the subject can be found in Refs. [4,5]. Early work on modelling AE wave propagation adopted analytical solutions from the field of geophysics using a method known as the Green's function. The Green's function describes the impulse dynamic response of the mechanical system. It is explained here using the partial differential equation for a homogenous isotropic

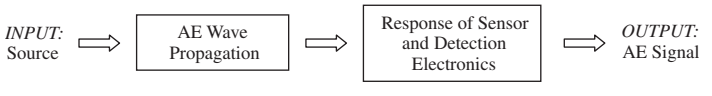

Fig. 1. A schematic diagram of an AE chain.

linear elastic solid. This equation treats displacement as unknown and is given by Höschl et al. [5]:

$$\mu u_{i,ll}(x,t) + (\lambda+\mu)u_{l,li}(x,t) + F_i(x,t) = \rho\ddot{u}_i(x,t), \tag{1}$$

where $u_i(x,t)$ and $F_i(x,t)$ are the displacements and body forces per unit volume at locations x and time t, μ and λ are Lamé constants, and ρ is the density. The time-dependent body forces model the source, and the displacement response is calculated from the equation. This equation represents a statement of dynamic equilibrium in each of the three orthogonal directions. Summation over repeated indices is used (e.g. $a_{ii} = a_{11} + a_{22} + a_{33}$). Commas represent partial differentiation with respect to space and dot notation indicates partial differentiation with respect to time. For wave motion excited by a unit impulse body force we can write Eq. (1) as [6]

$$\begin{aligned}&\mu G_{ij,ll}(x;x',t-t') + (\lambda+\mu)G_{lj,li}(x;x',t-t') + \delta_{ij}\delta(x-x')\delta(t-t')\\ &\quad = \rho\ddot{G}_{ij}(x;x',t-t'),\end{aligned} \tag{2}$$

where $G_{ij}(x;x',t-t')$ is the dynamic elastic Green's tensor. It is the displacement response in the i direction at (x,t) due to a unit impulse body force acting in the j direction concentrated at (x',t'). $\delta(x-x')$ and $\delta(t-t')$ are the Dirac delta functions and δ_{ij} is the Kronecker delta. The Green's tensor can be used to determine the displacement response $u_i(x,t)$ at (x,t) due to the application of arbitrary body forces $F_j^A(x',t')$ at (x',t') by

$$u_i(x,t) = \int_V \int_0^t G_{ij}(x;x',t-t')F_j^A(x',t')\,\mathrm{d}t'\,\mathrm{d}V. \tag{3}$$

As formulated above, the problem is a linear one and the response of a distributed source in space can be determined by superposing the convolution of each and every time-dependent point source in a volume V with its corresponding Green's function (i.e. between all source points and the receiver, Fig. 2).

Analytical expressions of the Green's function have been derived for a number of linear elastic bodies, including an infinite space, an infinite half-space, an infinite layered half-space and a plate with infinite lateral dimensions [7]. Exact solutions have been calculated using the generalised ray method [8]. These solutions are very accurate and were used for the calibration of AE sensors [9] and for the characterisation of AE sources in carefully designed experiments [10]. Nonetheless, obtaining analytical solutions for more complicated geometries or material properties becomes mathematically intractable.

2.3. The finite element method

Over the past decade, the traditional emphasis on analytical approaches for the analysis of wave propagation has shifted towards the development of sufficiently accurate numerical methodologies. The FE method is one of the most commonly used methods and has been applied for modelling AE by a number of authors [11–16]. It is based on exact theory and provides very accurate solutions. The FE method has the advantage of modelling structural geometries and material properties that do not have closed-form analytical solutions. Sources can be modelled with relative ease and AE responses for long

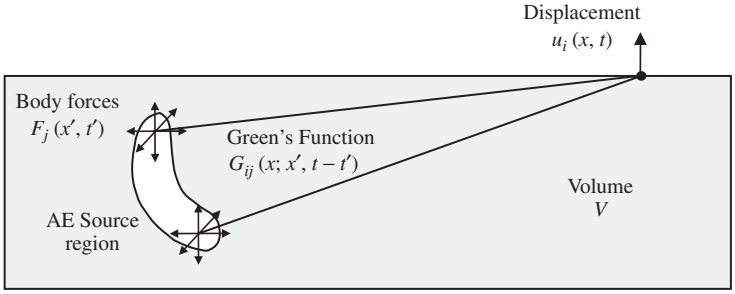

Fig. 2. A representation of the displacement response for a volume containing a distribution of body forces having finite time dependence (convolution of each and every time-dependent body force with its corresponding Green's function is superposed to arrive at the desired location).

signal durations can also be predicted. However, these advantages come at a cost of increased analysis time and computational resources.

The FE method is based upon the process of semi-discretisation, where the spatial domain is divided into finite elements connected at nodes. This procedure reduces the partial differential equations of continuum to a system of ordinary differential equations in time. The system is then solved in time using various time integration methods, leading generally to a system of algebraic equations. The general form of the equation solved in a dynamic transient FE analysis is as follows:

$$\mathbf{M}\ddot{\mathbf{u}} + \mathbf{C}\dot{\mathbf{u}} + \mathbf{K}\mathbf{u} = \mathbf{F}, \tag{4}$$

where $\mathbf{M}$ is the mass matrix, $\mathbf{C}$ is the damping matrix, $\mathbf{K}$ is the stiffness matrix, $\ddot{\mathbf{u}}$ is the nodal acceleration vector, $\dot{\mathbf{u}}$ is the nodal velocity vector, $\mathbf{u}$ is the nodal displacement vector, and $\mathbf{F}$ the load vector.

No physical damping has been considered in the analysis presented in this paper (i.e. the damping term is set to zero). A general purpose FE code (ANSYS) is used for the numerical analysis in this work. Eq. (4) is solved using an implicit Newmark time integration method at discrete time points (Δt). The details of the solution method can be found in the ANSYS Theory in Ref. [17]. The Newmark parameters α and δ are selected in accordance with the expressions:

$$\alpha = \tfrac{1}{4}(1+\gamma)^2, \tag{5}$$

$$\delta = \tfrac{1}{2} + \gamma, \tag{6}$$

where the amplitude decay factor is $\gamma \geqslant 0$. This gives an unconditionally stable solution. All the analysis reported in this paper is based on a value of 0.005 for γ. This introduces a small amount of numerical damping which can be viewed as desirable, since the FE solution often contains high-frequency components that are mere artefacts of the solution that have no physical meaning.

The spatial resolution of the FE method is an important parameter for achieving accurate results. It is selected according to the following equation:

$$\Delta l = \frac{\lambda_{\min}}{R}, \tag{7}$$

where Δl is the finite element size, $\lambda_{\min}$ is the minimum wavelength of interest and R is a resolution factor. A range of values between 10 and 20 is recommended for R in different references [11,13]. The minimum wavelength is given by

$$\lambda_{\min} = \frac{c_R}{f_{\max}}, \tag{8}$$

where $f_{\max}$ is the maximum frequency of the source and c_R is the Rayleigh wave velocity which is the slowest travelling wave and can be approximated as [18]

$$c_R \simeq \frac{c_S(0.87 + 1.12\nu)}{1+\nu}, \tag{9}$$

where ν is Poisson's ratio and c_S is the secondary wave velocity. For completeness:

$$c_S = \sqrt{\frac{\mu}{\rho}}, \tag{10}$$

where μ is shear modulus. The temporal resolution (Δt) of the FE method also affects the accuracy of the numerical solution. It is selected as the time required for the primary wave to traverse one element. This can be expressed as

$$\Delta t = \frac{\Delta l}{c_P}, \tag{11}$$

where c_p is the primary wave velocity given by the expression:

$$c_P = \sqrt{\frac{B + (4/3)\mu}{\rho}} \tag{12}$$

and B is the Bulk modulus.

2.4. The numerical band-limited Green's function

In order to evaluate the Green's function using the FE method, a unit impulse delta function force needs to be applied in the analysis. However, this would result in high frequency numerical errors. This is due to the fact that a delta function has an infinite bandwidth while the FE method is limited in frequency due to discretisation. Nonetheless, real AE sources and AE sensors are also bandwidth limited. Therefore, it suffices to compute using the FE method a band-limited Green's function by applying a band-limited approximation of an impulse delta function. Using Eq. (4) the band-limited Green's function can be expressed as

$$\mathbf{M}\hat{\ddot{\mathbf{G}}} + \mathbf{C}\hat{\dot{\mathbf{G}}} + \mathbf{K}\hat{\mathbf{G}} = \mathbf{F}^{\mathbf{I}}, \tag{13}$$

where $\mathbf{F}^{\mathbf{I}}$ is a band-limited approximation of a unit impulse delta function applied in the j direction at (x', t'). In this work, the Hanning function is selected to approximate a delta function. The Hanning function is a smooth function and has most of its energy concentrated in a bandwidth of interest. This is useful since there is less energy in the wavelengths that are smaller than the element size of the FE model and hence less numerical errors should be observed.

The Hanning function is defined by the expression:

$$F^I(t) = \begin{cases} \cos^2\left(\frac{\pi(t-\tau)}{2\tau}\right) \times \frac{1}{\tau}, & 0 < t \leqslant 2\tau, \\ 0, & t > 2\tau, \end{cases} \tag{14}$$

where τ is half the pulse width. As formulated above, the pulse peak is $1/\tau$, which gives an area of unity (Fig. 3). The maximum frequency of the band-limited Green's function solutions and the FE model was defined at -3 dB of the magnitude spectrum of the Hanning function.

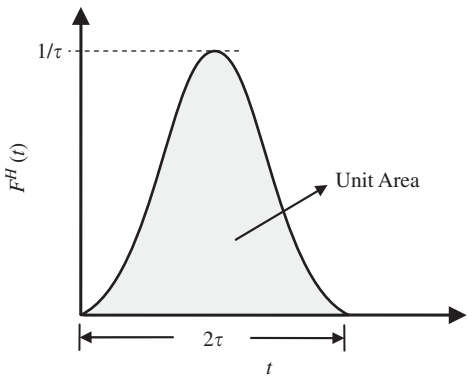

Fig. 3. Hanning function; used to estimate a bandwidth limited Dirac delta function.

The band-limited Green's function can be written in terms of the complete Green's function using

$$\hat{G}_{ij}(x;x',t-t') = \int_0^t G_{ij}(x;x',t-t')F_j^I(t')\,\mathrm{d}t'. \tag{15}$$

The displacement response due to the application of an arbitrary time-dependent body force $F_j^A(x',t')$ in the j direction at (x',t') can be calculated using the band-limited Green's function as

$$\hat{u}_i(x,t) = \int_V \int_0^t \hat{G}_{ij}(x;x',t-t')F_j^A(x',t')\,\mathrm{d}t'\,\mathrm{d}V. \tag{16}$$

Note that $\hat{u}_i(x,t)$ is band-limited and delayed in time by half the pulse width (τ) of the Hanning function. It is related to the complete displacement response by

$$\hat{u}_i(x,t) = \int_0^t u_i(x,t-t')F^I(t')\,\mathrm{d}t'. \tag{17}$$

2.5. The reciprocity theorem

Most of the work reported on the use of FE method for AE analysis has been carried out using an approach whereby every FE analysis provides the AE displacement responses at all points in the discretised space due to the application of one specific loading condition (i.e. unique source). This is inefficient since for AE analysis it is most useful to be able to predict the AE response at one receiver location but for multi-source locations. Here it is proposed to apply the reciprocal relationship between the source and the receiver to enable the use of the FE method more efficiently for multi-source simulation.

The reciprocity theorem states that one can calculate the same waveform if the direction and location of the source and receiver are interchanged. Theoretical proof of the reciprocity theorem can be found for different materials and boundaries in Ref. [19]. The reciprocal relation is expressed using the Green's function as follows:

$$G_{ij}(x;x',t-t') = G_{ji}(x';x,t-t'). \tag{18}$$

By applying the force at the location of the receiver and in the direction of the measurement response of the AE sensor, the band-limited Green's function for all points in the discretised space relative to one AE sensor can be calculated from only one FE simulation. The AE response for any force distribution in space and/or time can then be simulated using the reciprocal band-limited Green's function solutions. Thus, the band-limited displacement response in Eq. (16) can be rewritten using the reciprocal band-limited Green's function as

$$\hat{u}_i(x,t) = \int_V \int_0^t \hat{G}_{ji}(x';x,t-t')F_j^A(x',t')\,\mathrm{d}t'\,\mathrm{d}V. \tag{19}$$

3. Analytical validation

In this section, the known analytical solutions of the exact Green's function are used to validate the FE solutions. The analytical solutions were computed using a computer program provided to the authors by Hsu [20]. The program computes the Green's function of an axi-symmetric elastic isotropic plate with infinite lateral dimensions.

A 6 mm glass plate was selected for this study. The material properties are specified in Table 1. The source was applied vertically at a point on the top surface of the plate. The results were computed at different point locations on the top and bottom surfaces and in both the vertical and horizontal directions. The duration of the analysis was 14 μs. Using Eq. (15), the calculated analytical solutions of the exact Green's functions were then convolved in time with the Hanning source function to evaluate an analytical band-limited Green's function. The bandwidth of the Hanning function used in the analysis was 2 MHz at −3 dB; this is equivalent to a pulse width of 0.36 μs.

Table 1
Mechanical properties of the glass plate

Material properties		Wave speed calculations (m/s)	
Poisson's ratio	0.23	Primary wave	5697.4
Density	2500 kg/m^3	Secondary wave	3373.7
Young's modulus	70 GPa	Rayleigh wave	3092.9

An equivalent two-dimensional FE model of the cross-section of the same plate used in the analytical calculations was created. However, the plate was finite in length with a radius of 78 mm. This radius was long enough not to include any reflections from the plate lateral surfaces from the fastest travelling wave (c_p) during the whole time of analysis. Linear solid axi-symmetric elements were used to mesh the plate. The elements consisted of 4-nodes with 2 degrees of freedom at each node. The size of every element was 0.06 mm (i.e. 100 elements across the plate thickness); this is equivalent to a value of more than 25 for the resolution factor (R) defined in Eq. (7) and is above the recommended value for R found in Refs. [11,13]. The FE model consisted of a total of 131,401 nodes. The time step of the FE analysis was 0.0105 μs, which satisfied the stability condition in Eq. (11). The same Hanning function source was applied vertically through the axis of symmetry at the node located on the top surface of the plate. The solutions were extracted at the same point locations that were computed analytically. The results are shown in Figs. 4 and 7.

Excellent agreement has been observed between the FE results and the analytical solutions. There are some high frequency numerical discrepancies in the results especially for the responses of the top surface. These errors can be minimised by increasing the resolution of the FE element method (Figs. 5–7).

4. The effects of the resolution of the FE method

In this study, the effects of varying the resolution factor (R) of the FE method are investigated in order to determine an optimum value for R that would provide accurate results without exhausting the computation resources. The same plate modelled in the previous section was used here. The source was applied at a point on the top surface and in the vertical direction. The bandwidth of the Hanning function source was 2 MHz. The band-limited Green's functions in the vertical direction were calculated at two receiver points on the plate; the first located at the top surface and the second was located at the bottom surface. Both points were two plate thicknesses away from the source (i.e. 12 mm). The duration of the analysis was 5.27 μs.

The analytical solutions of the band-limited Green's function were calculated using the same program provided by Hsu [20] and in the same way as described in the previous section. Ten FE simulations using different resolution factors were computed. The element lengths were calculated using Eq. (7) for values of R between 5.7 and 57.5. For every FE simulation, the time step size was calculated with respect to the element length using Eq. (11).

The results are shown in Figs. 8 and 9. As the resolution is increased the FE solutions converge with the exact analytical solutions. The numerical solutions at the bottom surface point location converged with lower resolution than the point at the top surface. This is because the displacement at the top surface point location has more energy in the higher frequencies than the response at bottom surface point location, thus requiring a higher resolution.

The results were analysed further to determine the correlation coefficients between the exact analytical solutions and the numerical ones for varying resolution factors. This provided a measure of convergence; a correlation coefficient of unity means that the signals are exactly the same, while zero indicates no correlation. The results of the correlation coefficients are plotted against R in Fig. 10 for both receiver locations.

It is important to note that the maximum frequency of the applied source affects the minimum wavelength of interest and hence the interpretation of the results. The analysis presented here is for a point source Hanning function with a maximum frequency defined at −3 dB. It is also important to note that different

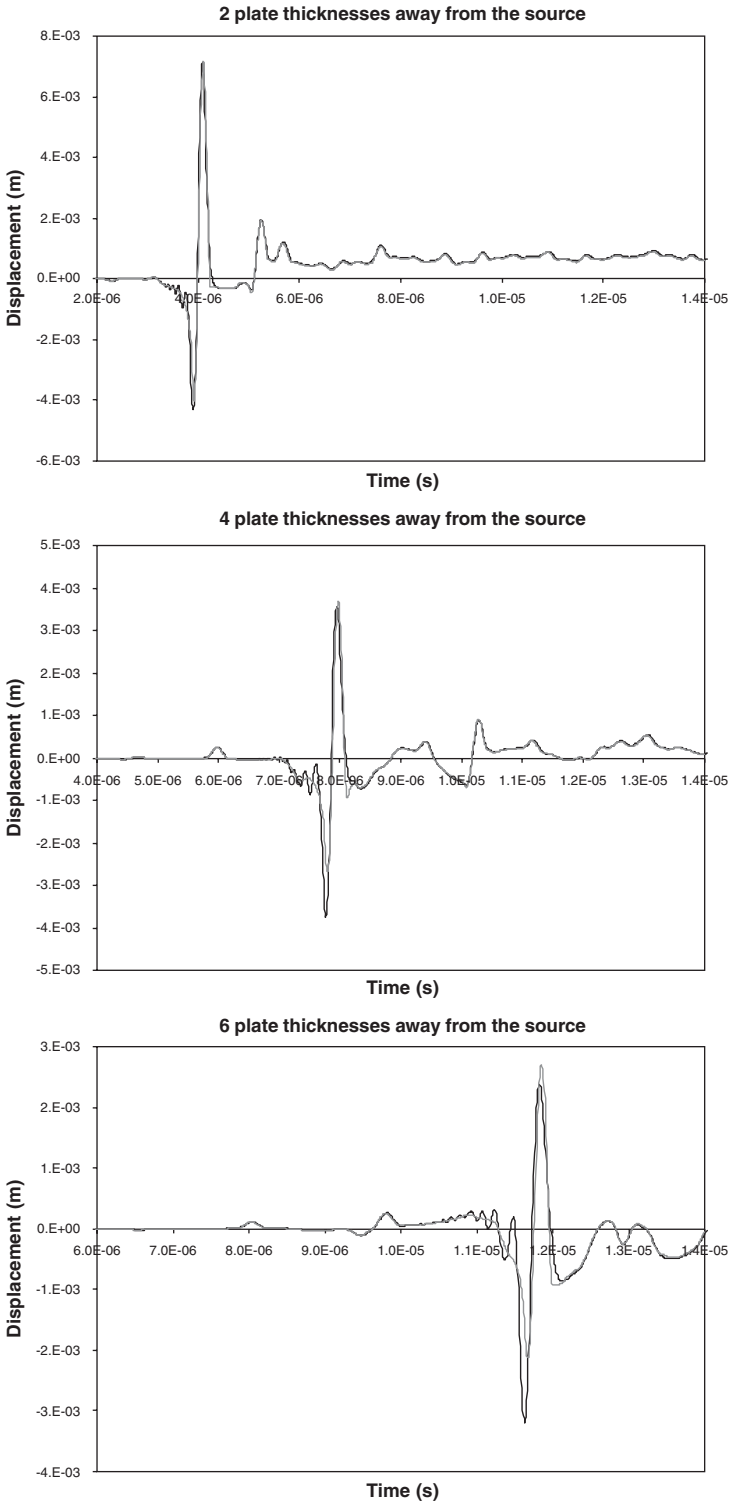

Fig. 4. FE (black line) and analytical (grey line) solutions of the band-limited Green's functions in the vertical direction at varying point locations on the top surface of a plate (the source was applied in the vertical direction at a point on the top surface of the plate).

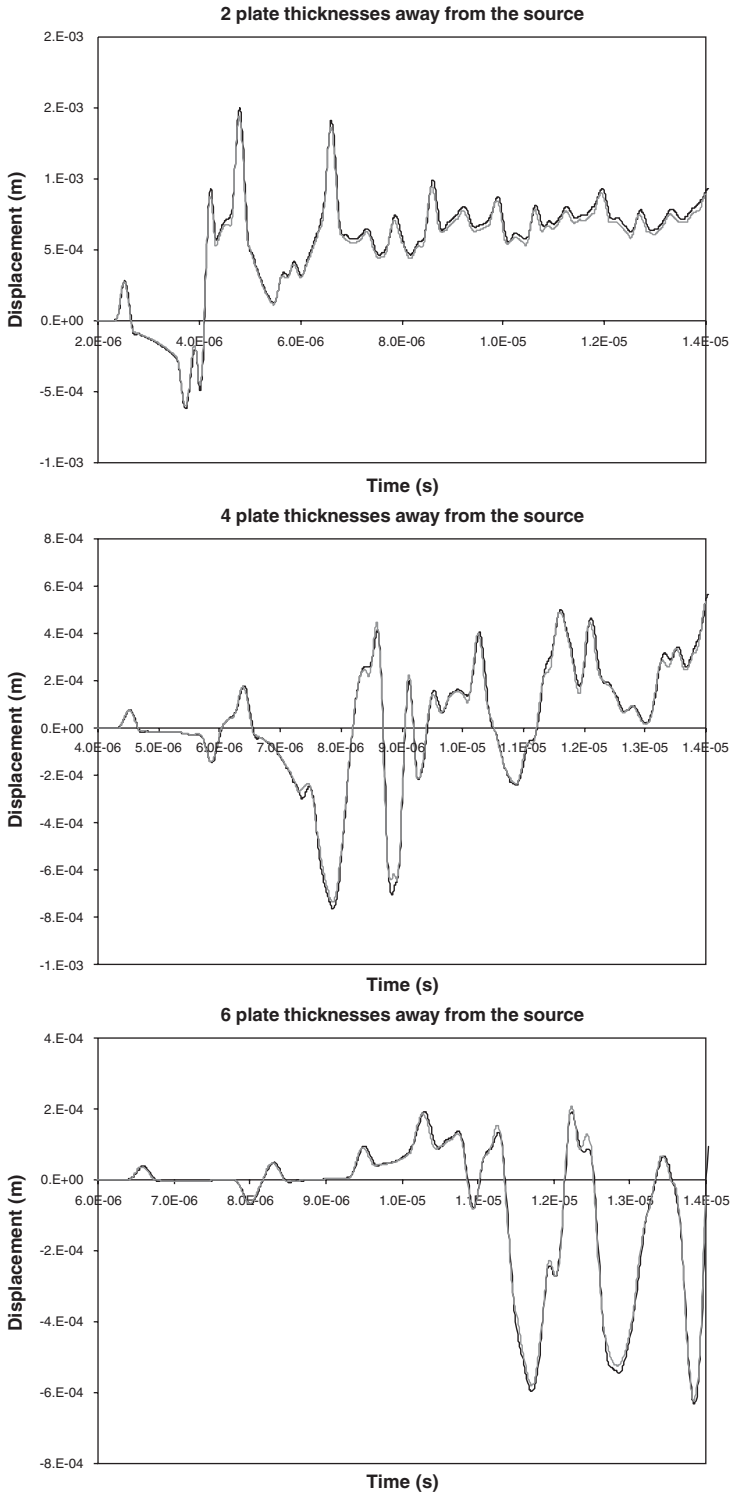

Fig. 5. FE (black line) and analytical (grey line) solutions of the band-limited Green's functions in the vertical direction at varying point locations on the bottom surface of a plate (the source was applied in the vertical direction at a point on the top surface of the plate).

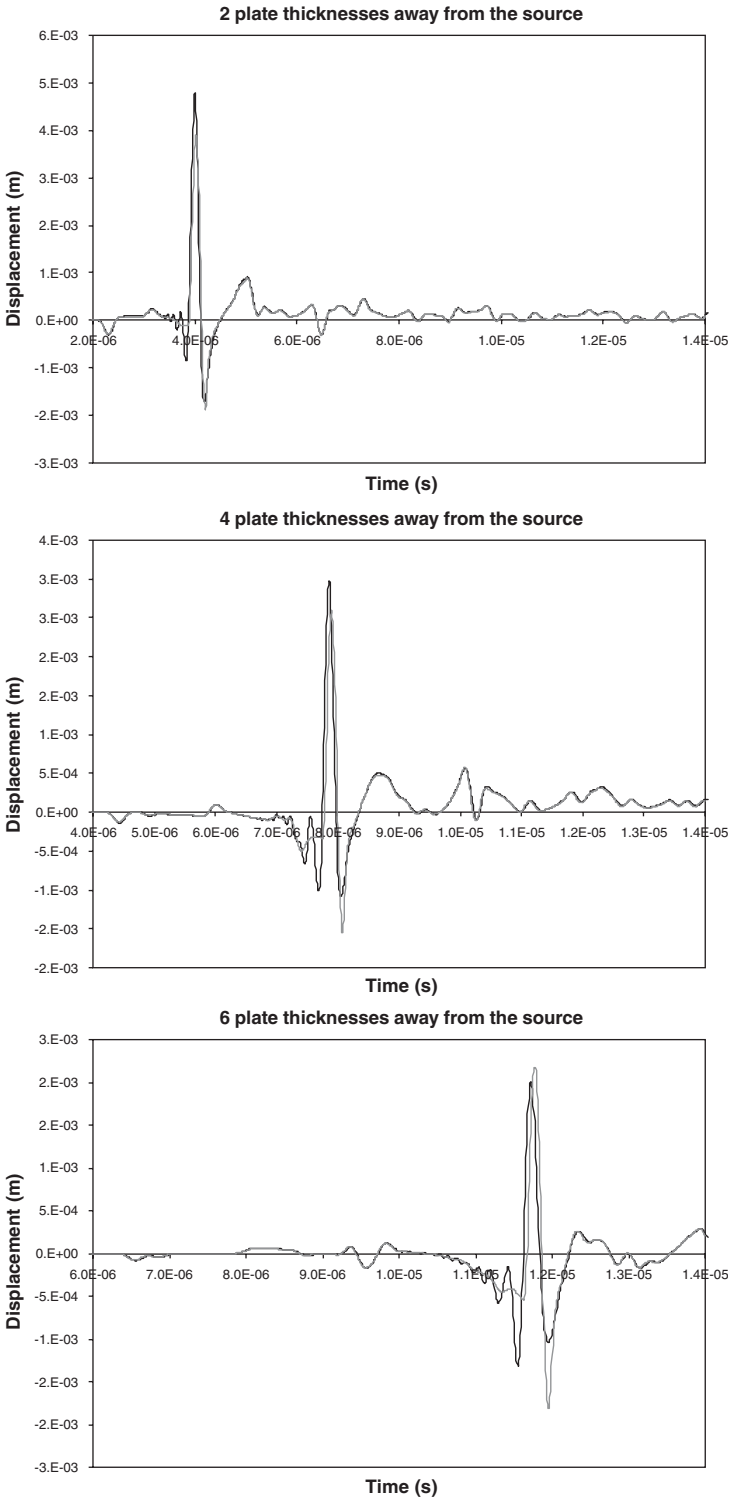

Fig. 6. FE (black line) and analytical (grey line) solutions of the band-limited Green's functions in the horizontal direction at varying point locations on the top surface of a plate (the source was applied in the vertical direction at a point on the top surface of the plate).

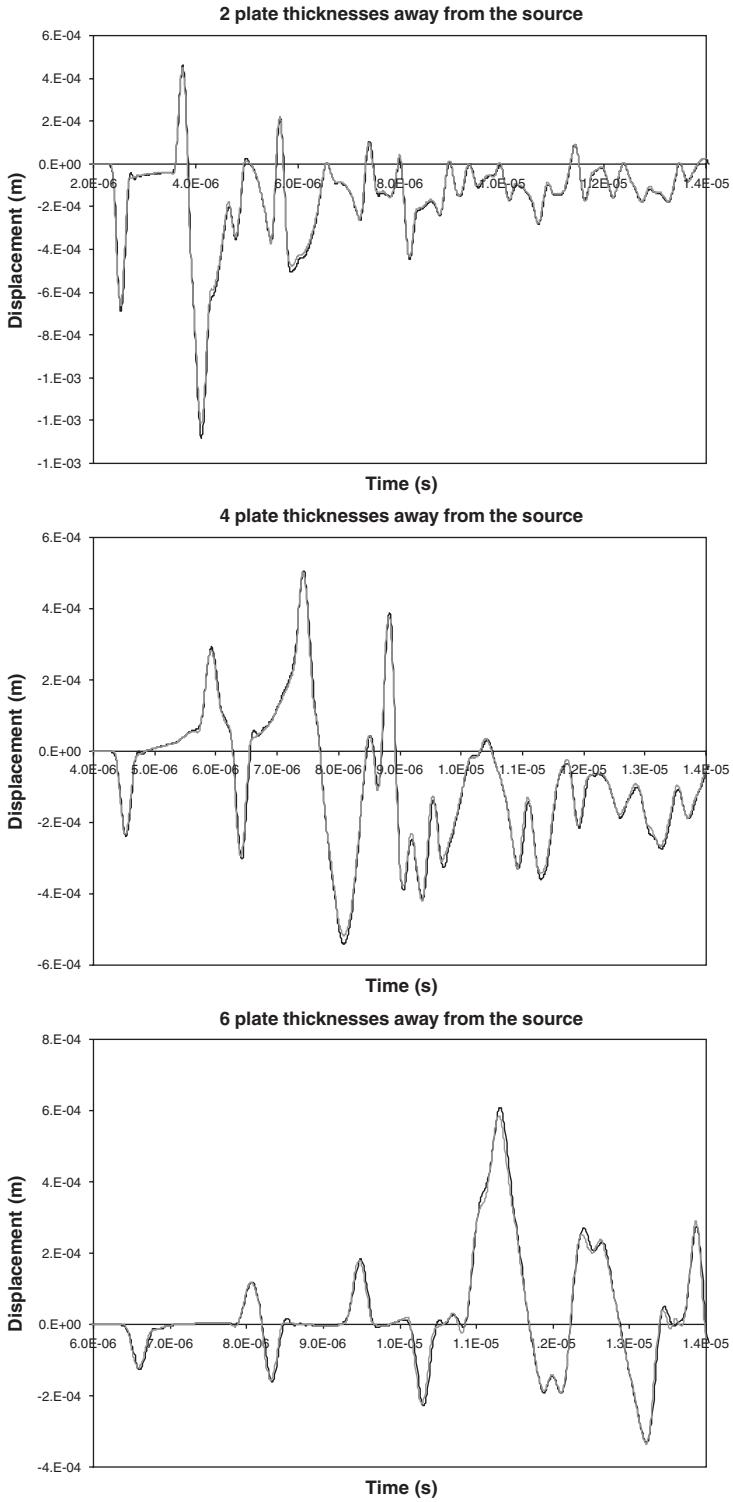

Fig. 7. FE (black line) and analytical (grey line) solutions of the band-limited Green's functions in the horizontal direction at varying point locations on the bottom surface of a plate (the source was applied in the vertical direction at a point on the top surface of the plate).

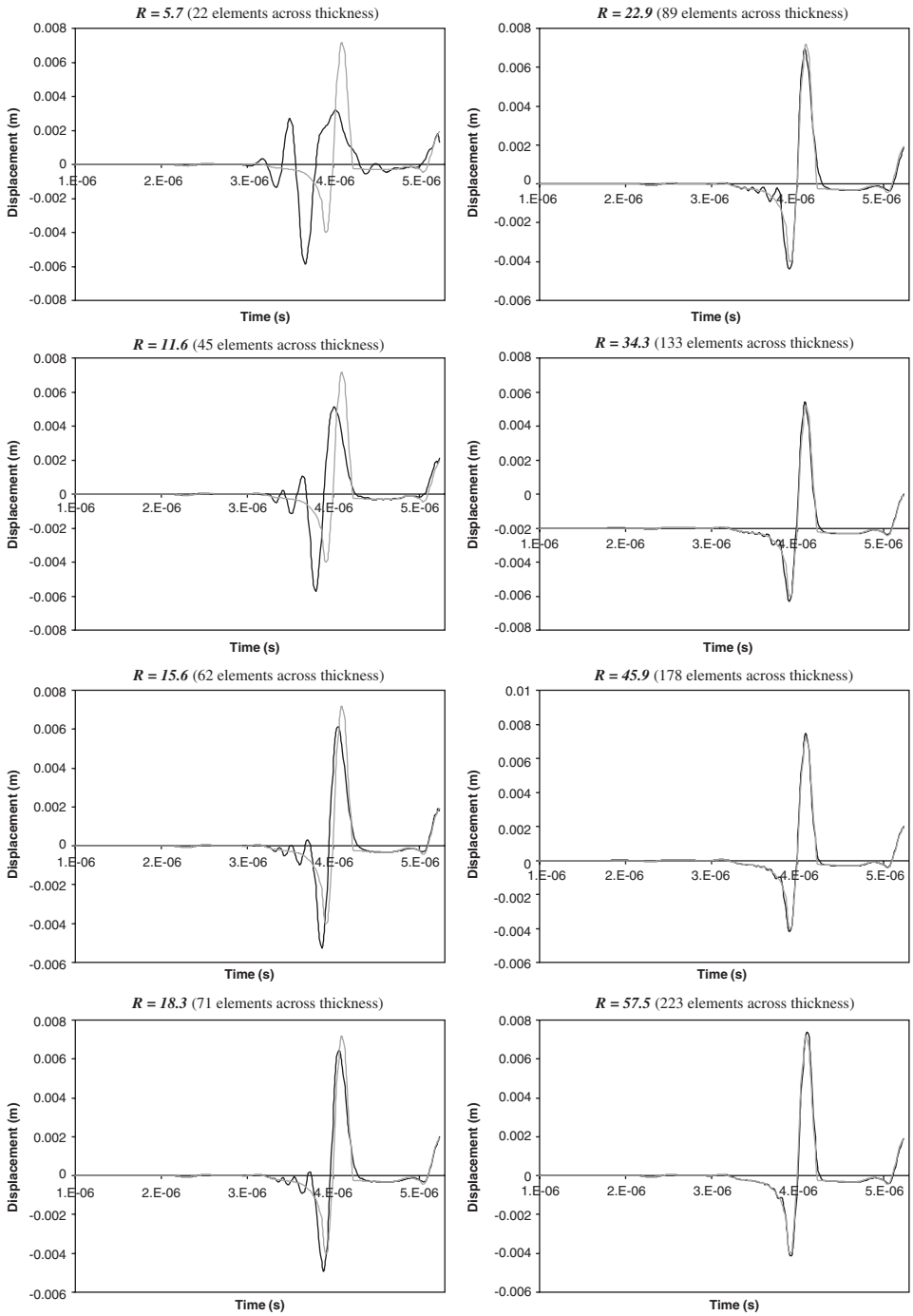

Fig. 8. FE (black line) and analytical (grey line) solutions of the band-limited Green's functions in the vertical direction at a point on the top surface of the plate and located two plate thicknesses away from the source. The source was applied at a point in the vertical direction on the top surface of the plate. Results are shown for different resolution factors (R).

geometries and/or source/sensor locations might require lower or higher resolutions. Therefore, this study is only a guideline for the selection of the resolution factor R when the proposed band-limited Green's function approach is used. The resolution can be selected based on a balance between the accuracy required and the computational resources that are available. In general, it can be said that a value below 15 for R is not

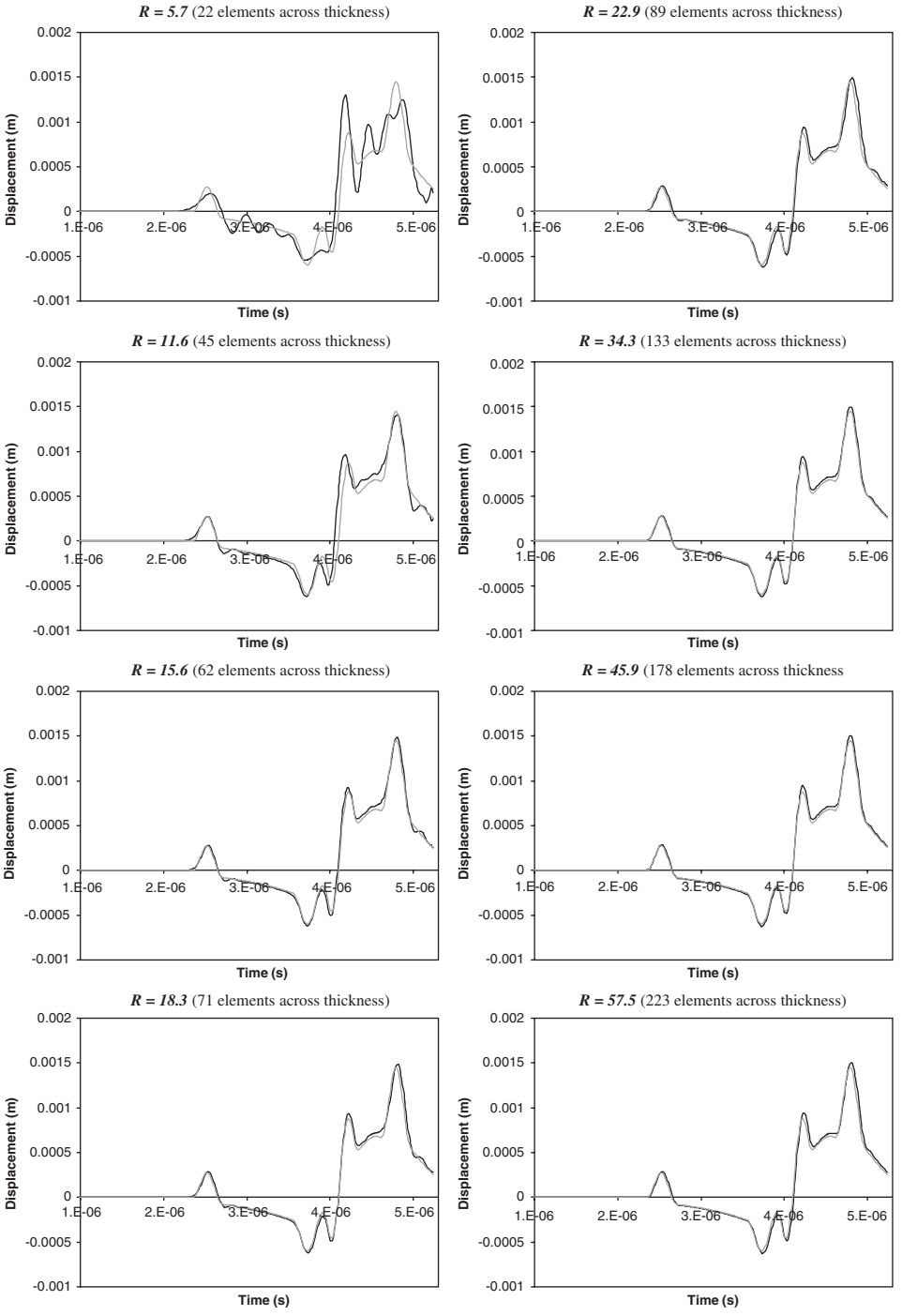

Fig. 9. FE (black line) and analytical (grey line) solutions of the band-limited Green's functions in the vertical direction at a point on the bottom surface of the plate and located two plate thicknesses away from the source. The source was applied at a point in the vertical direction on the top surface of the plate. Results are shown for different resolution factors (R).

recommended as the numerical errors become too high, while any value above 30 for R is a waste of computation power since the numerical solutions become almost identical to the exact analytical solutions (correlation coefficient above 0.99).

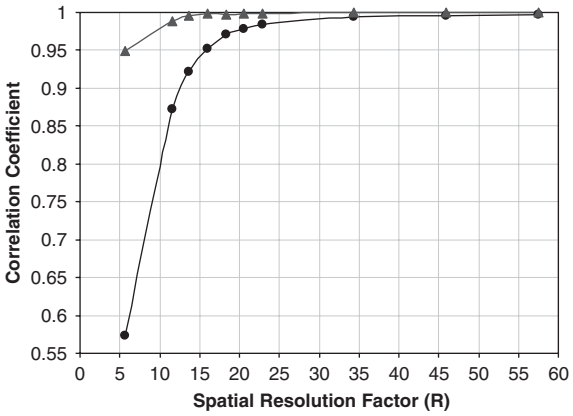

Fig. 10. Correlation coefficients between the analytical and FE solutions for varying resolution factors (R). Circles represent the results for the top surface and triangles represent the results for the bottom surface of the plate.

5. Experimental validation

In the previous sections, only near-field AE responses and short signal durations have been studied. In this section, AE measurements are used to validate the AE responses for receiver locations up to 70-plate thickness away from the source and for analysis duration of 150 μs. Two known artificial AE sources have been used: ball impact and pencil lead-break sources. Both sources are axisymmetric and can be considered as point sources since the source size is much smaller than the minimum wavelength.

A circular glass plate with a diameter of 1 m and thickness of 6 mm was selected for this study. The manufacturer's material properties are given in Table 1. The reason for choosing glass for the experiment was due to the fact that it has a very homogeneous microstructure with small variation in thickness along its diameter; this reduces errors between the FE model and the experimental results. The glass was supported on 10 mm wide rubber bars which were glued on a stable table, as shown in Fig. 11. Rubber was used to absorb any background AE from the surrounding. The artificial AE sources were applied at the centre of the plate and measurements were taken at different locations away from the source along a straight line (line A–B in Fig. 11).

A high-fidelity conical piezoelectric sensor [21] was used to measure the generated displacement responses. The small contact tip of the sensor compared to the minimum wavelength over the frequency range of interest (nominally up to 1 MHz) makes the sensor an approximation to a point detector. The sensor has a relatively flat frequency response from 50 kHz to 1 MHz. A 60 dB pre-amplifier and 0.2–1.2 MHz analogue filtering was applied to the raw signals before they were recorded on a computer using a 10 MHz sampling rate high-speed data acquisition card (National Instruments).

A two-dimensional axi-symmetric FE model of the cross-sectional area along the line A–B was modelled. The source was applied vertically on the top surface along the axis of symmetry. It was applied on one element (i.e. 2 nodes). The finite size of the source is much smaller than the minimum wavelength of interest and can therefore be considered as a point. At the same time the band-limit of the source in space could help reduce high-frequency numerical errors [15,16]. Zero displacement initial conditions were applied at the rubber support points (as shown in Fig. 11). The maximum frequency of the applied Hanning source function was 1 MHz. Forty-five elements across the plate thickness were used; this is equivalent to a spatial resolution factor of 23.2 (i.e. 0.133 mm element size). A totao of 172,546 nodes were needed to mesh the geometry. The solutions were solved for 6410 time steps; every time step was 0.0234 μs.

The first source investigated in this analysis was the ball impact source [22,23]. From Hertz contact theory, the contact duration t_d for a ball impacting a large flat stationary solid surface with an impact velocity c_1 is

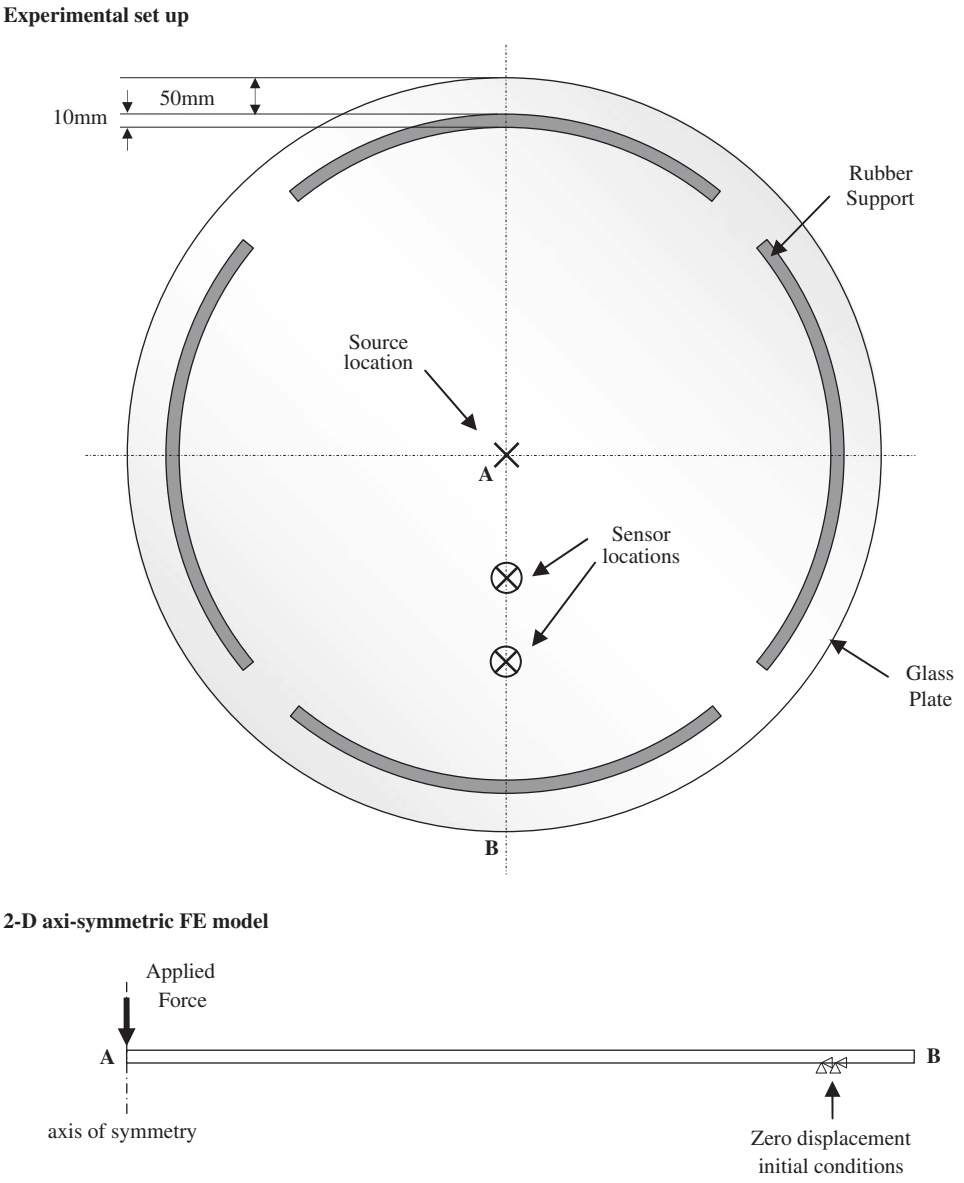

Fig. 11. The experimental set-up and the equivalent two-dimensional axi-symmetric FE model.

given by Timoshenko and Goodier [24]

$$t_d = 2.94(a/c_I), \tag{20}$$

where a is the maximum distortion (displacement units) and is given by

$$a = \left(\frac{5v_i m}{4n}\right)^{2/5}, \tag{21}$$

where m is the mass of the ball and n is given by

$$n = \sqrt{\frac{16}{9\pi^2}\frac{r}{(k_g + k_s)^2}} \tag{22}$$

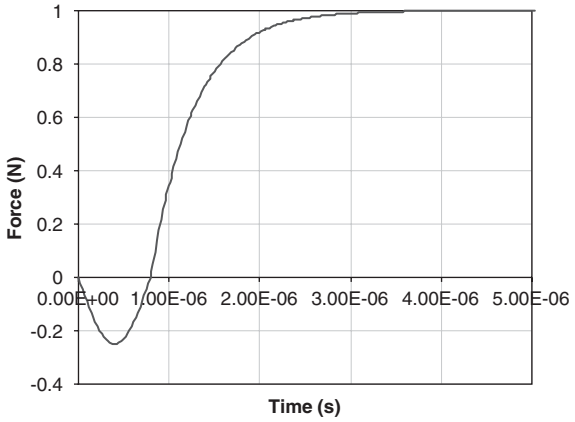

Fig. 12. Temporal characteristics of a pencil lead-break source; force amplitude = 1 N [25].

and r is the radius of the ball. k_g and k_s are material constants for the glass plate and the steel ball, respectively, and are given by the expression:

$$k = \frac{1 - v^2}{\pi E}, \tag{23}$$

where E is the Young's modulus.

In the experiments a 1 mm diameter stainless steel ball was used ($E = 120$ GPa and $v = 0.3$). The ball (mass 4 mg) was dropped from a height of 24 mm above the glass plate; a vacuum device was used to hold the ball above the surface of the plate and once the air pump was switched off the ball was dropped. This method was very repeatable. The contact duration of the ball was calculated using the Hertzian model to be 5.72 μs. A Hanning function was used to approximate the ball impact source function which had a pulse duration equal to the calculated ball impact contact duration [10].

The second artificial source used was the ASTM976 standard pencil lead-break source; 2 H 0.3 mm lead was used. Fig. 12 shows the temporal characteristics of the pencil lead-break source [25]. The repeatability of the pencil lead-break AE source was investigated at one sensor location and in general it was less repeatable than the dropping ball AE source.

The numerical displacement responses of the band-limited Green's function were taken in the normal direction (out-of-plane) at the locations of the sensor. The solutions were then convolved with the predicted theoretical function for the ball impact source and with the known source function of the pencil-break source. A digital Chebyshev type-1 fifth-order band-pass filter (20 kHz–1.2 MHz) was applied to the numerical signals to model the analogue filtering used in the experimental measurements. Another 50 kHz high-pass digital filtering was applied to both the numerical and experimental signals using Chebyshev type-1 fifth order filtering in order to remove the 'non-flat' frequency characteristic response of the conical sensor below 50 kHz frequency. Both numerical and experimental signals were then normalised in amplitude so that the two signals could be compared. The results for the ball impact source are shown in Fig. 13 and those for the pencil lead-break source are shown in Fig. 14.

In general the experimental results are in very good agreement with the numerical predictions. However, the ball impact results are in better agreement than the pencil lead-break results. One explanation for this is that the model of the ball impact source is more accurate than the model used for the pencil lead-break source. Another reason for the discrepancies could be due to the fact that the pencil lead-break AE source is higher in frequency than the ball impact AE source. The maximum frequency of the numerical band-limited Green's function was 1 MHz.This might not have been high enough to convolve the high frequency response of the pencil lead-break source. This problem can be resolved by increasing the bandwidth of the Hanning function to obtain a wider bandwidth for the numerical band-limited Green's function. Other sources of error are due to variations in the plate thickness and also ringing in the sensor.

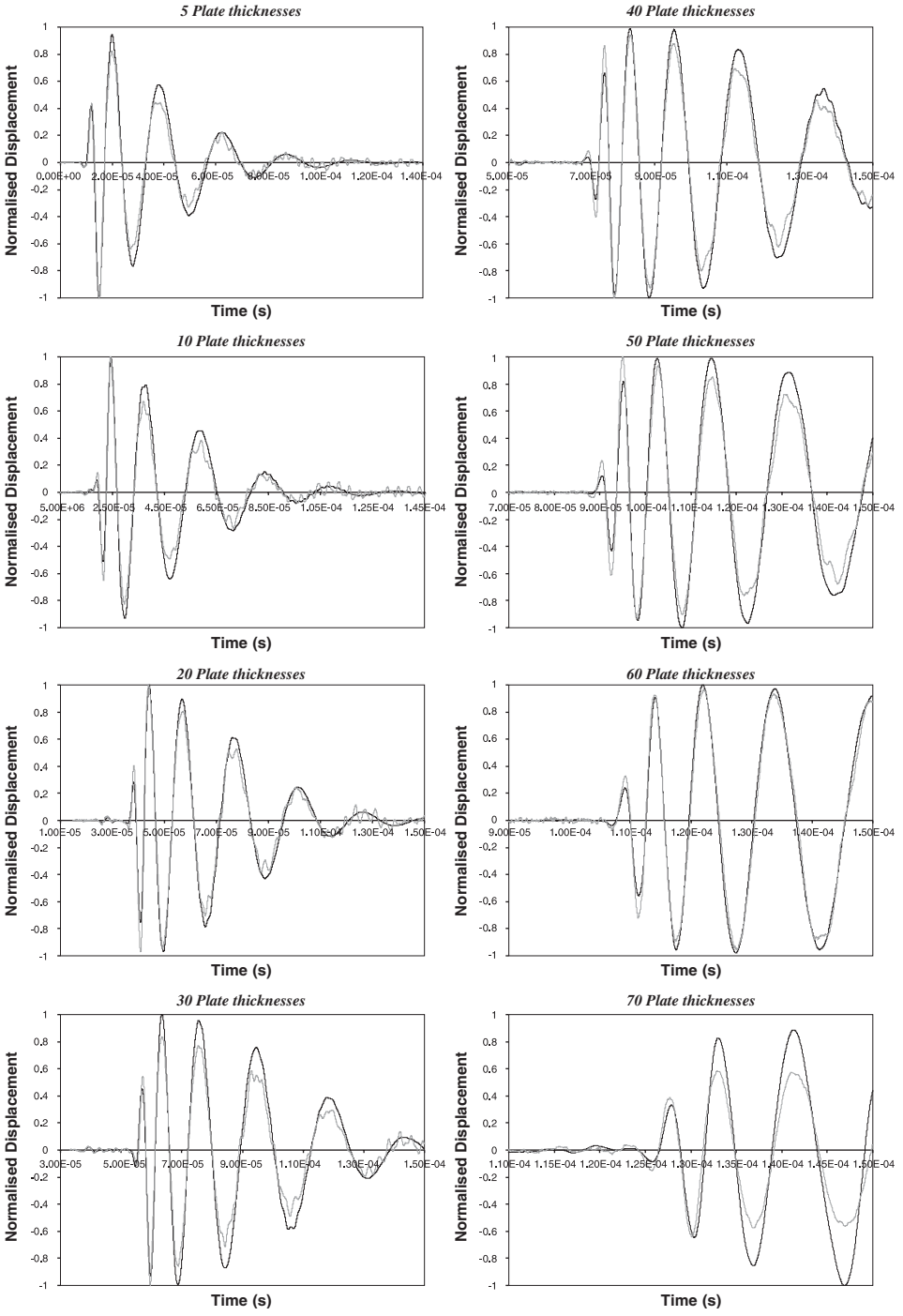

Fig. 13. Comparison between FE (black line) and experimental (grey line) AE responses for a ball impact source at varying locations from the source.

6. Source–receiver reciprocity

A plane stress model of an elastic isotropic plate was used to demonstrate the reciprocal relation between the source and the receiver. The material properties of the plate are shown in Table 1. The modelled cross-

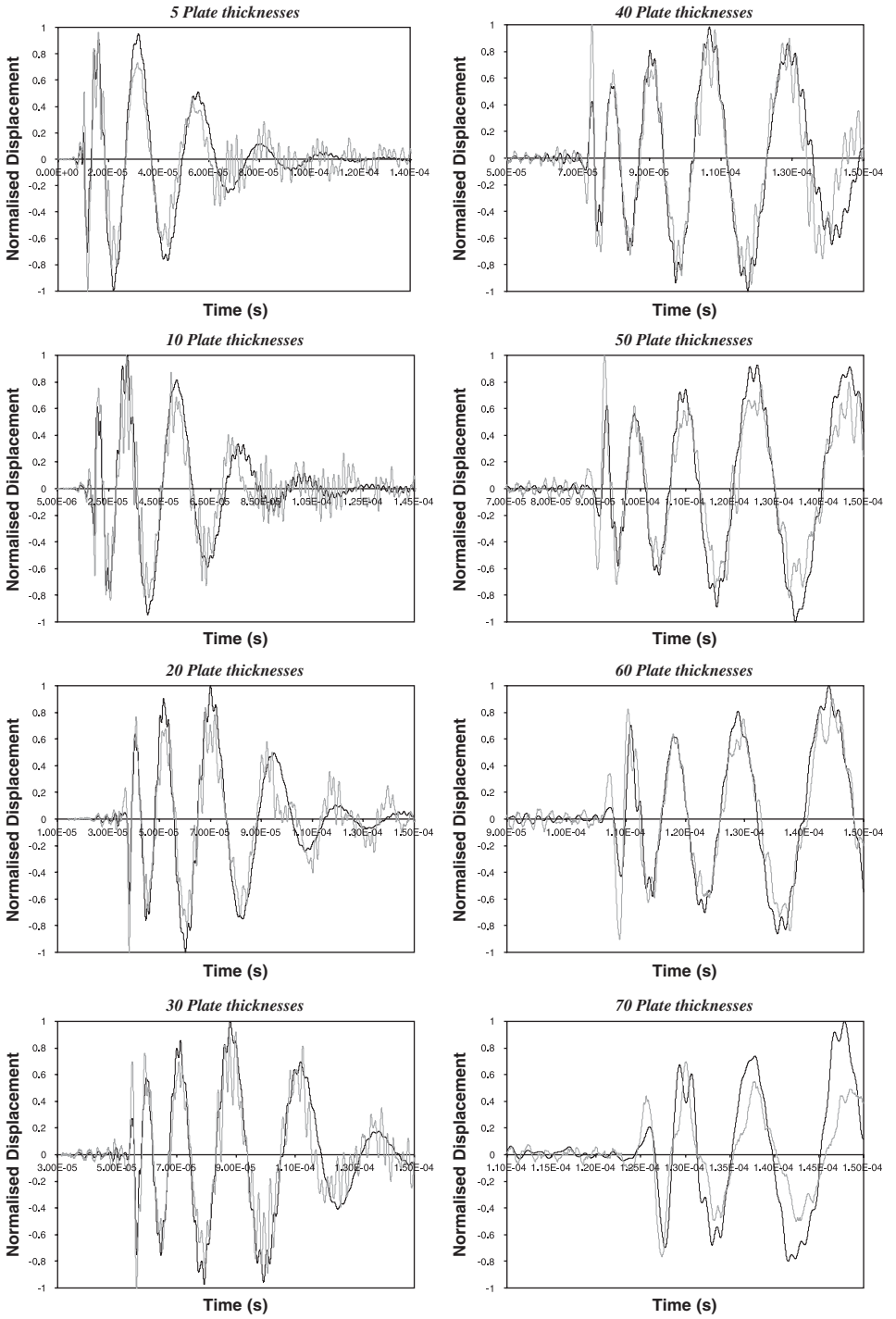

Fig. 14. Comparison between FE (black line) and experimental (grey line) AE responses for a pencil lead break source at varying locations away from the source.

section of the plate was 6 mm thick and 30 mm long. The analysis was conducted using two-dimensional first-order 4-node plane-stress elements. The plate was modelled using 60 elements across the thickness (i.e. 0.1 mm size of each element). This is equivalent to a resolution factor (R) larger than 15 for a Hanning function source

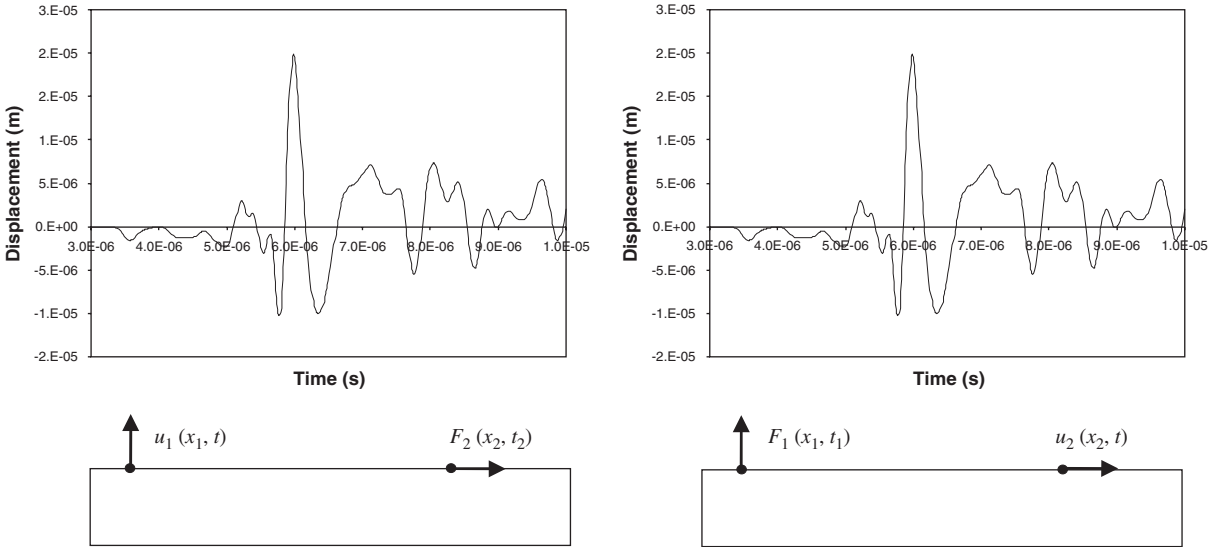

Fig. 15. Numerical solutions of the band-limited Green's function for a plane stress analysis of a plate. The plot on the left shows the displacement response of the surface at point x_1 in the 1-direction due to a point source applied on the surface at point x_2 in the 2-direction. The same displacement response is obtained (right) when the source and the receiver are interchanged.

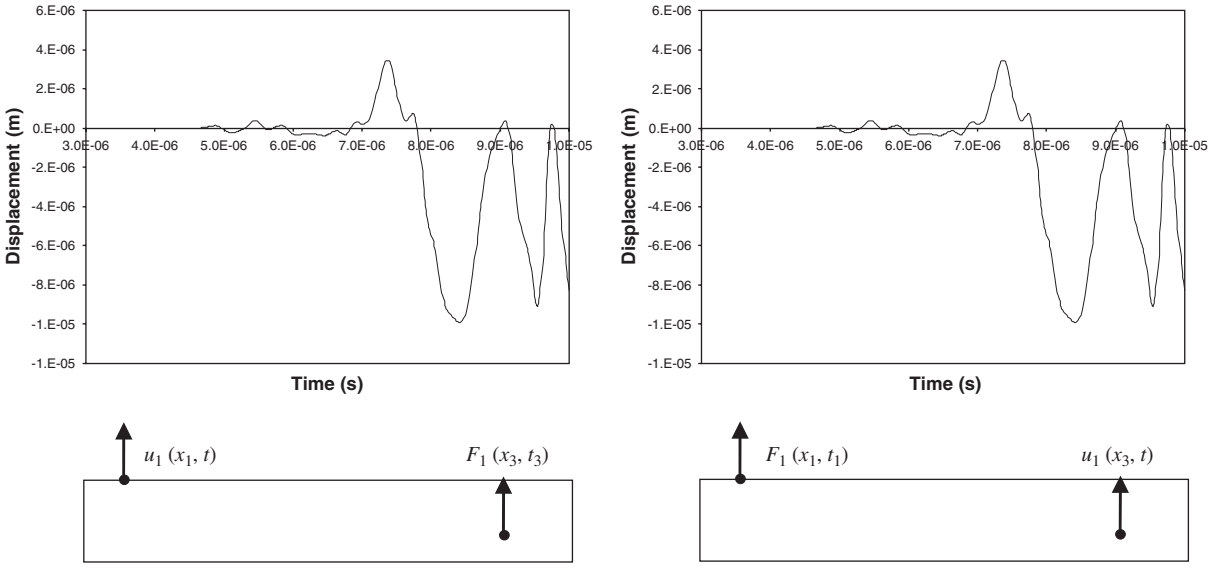

Fig. 16. Numerical solutions of the band-limited Green's function for a plane stress analysis of a plate. The plot on the left shows the displacement response of the surface at point x_1 in the 1-direction due to a point source applied internally at point x_3 in the 2-direction. The same displacement response is obtained (right) when the source and the receiver are interchanged.

with a maximum frequency of 2 MHz at −3 dB of the magnitude spectrum. This Hanning function source was used to model the source for all the analysis presented in this section. The analysis was conducted for 10 μs using 570 time steps.

The reciprocal relation between two points, x_1 and x_2, was first investigated. Taking the origin at the bottom left corner of the plate, the horizontal coordinates of the two points were 3 and 21 mm, respectively. Both points were located at the top surface (i.e. vertical coordinate 6 mm). In the first FE simulation the source

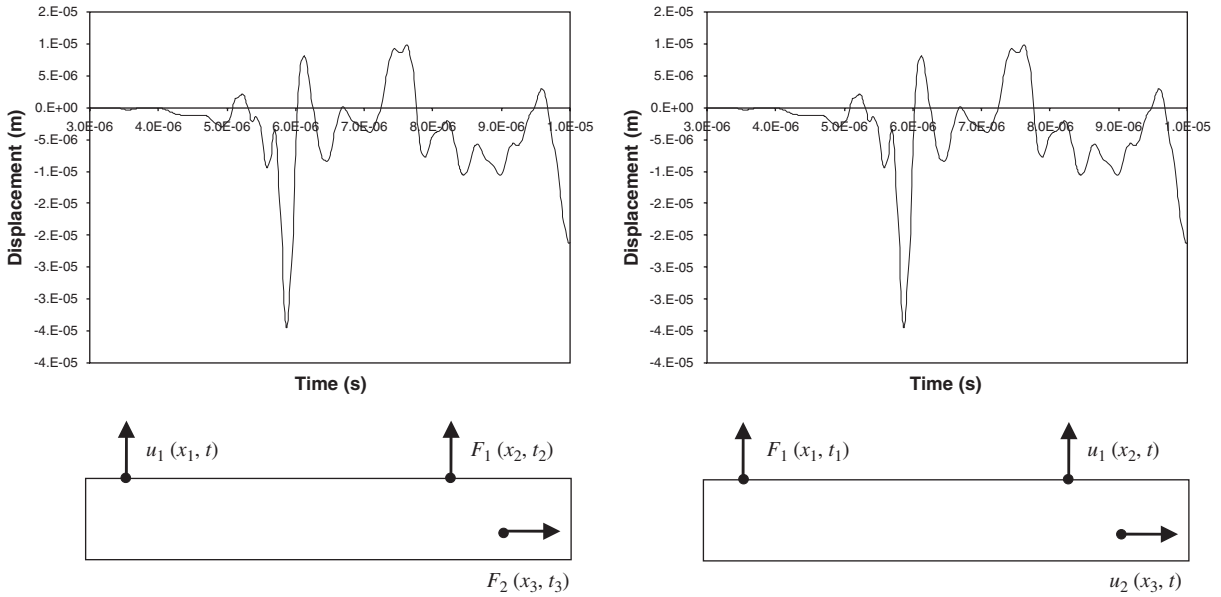

Fig. 17. Numerical solutions of the band-limited Green's function for a plane stress analysis of a plate. The plot on the left shows the displacement response of the surface at point x_1 in the 1-direction due to a distributed source applied at two points, x_2 and x_3 as shown in the diagram. The same displacement response is obtained (right) when the source and the receiver are interchanged and the displacement responses are superposed.

was applied at point x_2 in the 2-direction and the displacement response was extracted at point x_1 in the 1-direction (1 represents vertical direction and 2 represents horizontal direction). In the second FE simulation the source and receiver locations and directions were interchanged. The directions and locations of the receiver and source for both FE simulations are shown in Fig. 15 along with the calculated displacement responses. It is demonstrated that exactly the same displacement response is obtained.

Another point was selected for the analysis, x_3, which was located internally 2 mm from the origin in the vertical axis and 28 mm from the origin in the horizontal axis. The reciprocal relation between x_1 and x_3 was investigated here. Fig. 16 shows the direction of the applied forces and calculated responses together with the displacement response results. Again exactly the same solution was obtained when the source and the receiver were interchanged.

Finally, the authors demonstrate how a distributed source in space can be modelled using the reciprocal Green's function approach. Here the displacement response is first calculated at point x_1 for a distributed force in space applied at locations x_2 and x_3. The directions of the applied forces and the calculated displacement response are shown in Fig. 17. By applying the force (source) at the location the receiver point x_1 and in the same direction of the calculated displacement in the previous analysis, it was possible to obtain exactly the same resultant displacement response by superposing the individual responses at points x_2 and x_3, as shown in Fig. 17. Therefore, the AE response at one sensor location can be calculated for any distribution of forces in space and/or time by superposing the individual reciprocal Green's functions calculated from every point source using only the results of one FE simulation.

7. Conclusion

An efficient approach for calculating the band-limited Green's functions using the FE method is reported here. The approach has been validated using known analytical solutions for an isotropic plate. The effects of the spatial resolution of the FE method have been investigated and some guidelines for the selection of resolution factor are presented. It is concluded that when the proposed numerical band-limited Green's

function is used to model isotropic homogeneous solids a resolution factor below 15 produces large numerical discrepancies, while no significant gains of accuracy are achieved at values higher than 30.

It has also been demonstrated how the approach can be used to convolve the response of two known AE point sources (pencil lead-break and ball impact). Good agreement has been observed between the numerical solutions and the AE measurements. Finally, the reciprocal relationship between the source and the receiver has been confirmed using numerical solutions for a plane stress model of an isotropic plate. It is pointed out how the theorem can be applied for modelling AE signals at a single receiver location due to multiple AE source types and source locations using the numerical solutions of only one FE simulation.

Although only two-dimensional axi-symmetric and plane-stress results have been investigated in this paper, the application of the approach to three-dimensional models is relatively straightforward. The proposed reciprocal band-limited Green's function approach is a powerful and efficient tool for modelling AE in cases the problem cannot be treated analytically or be controlled experimentally. The proposed approach can also enhance the understanding of the AE phenomenon and lead to the development of more robust and reliable AE monitoring systems with lower costs.

This work is part of a larger project which investigates the propagation of AE in fibre reinforced composites. The principles of the proposed approach will be used to simulate AE signals due to different damage mechanisms in composite samples. AE measured from carefully designed experiments will be used for validating the model of the AE source (i.e. damage mechanism) as well as the model of wave propagation in composite materials. Once this is done, the method can be used for simulating AE from known damage mechanisms at grid of locations for the structure of interest. The simulated AE signals can then be processed further using advanced signal processing tools and classification technology to identify features of the AE signals that are related to composite damage mechanisms. The analysis can also consider the effects of source location on the AE signal features. This would allow the development of more reliable AE monitoring systems that are superior to systems developed using experimental AE data.

Acknowledgements

The authors gratefully acknowledge the financial support of the National Physical Laboratory. The authors would also like to acknowledge Nelson Hsu for his advice and for providing the program for calculating the analytical solutions of the Green's function of a plate.

References

[1] R.V. Williams, *Acoustic Emission*, Hilger, Bristol, 1980.
[2] R. Burridge, L. Knopoff, Body force equivalents for seismic dislocations, *Bulletin of the Seismological Society of America* 54 (1964) 1875–1914.
[3] N.N. Hsu, Characterization and calibration of acoustic emission sensors, *Materials Evaluation* 39 (1981) 60–68.
[4] K.F. Graff, *Wave Motion in Elastic Solids*, Clarendon Press, Oxford, 1975.
[5] C. Höschl, M. Okrouhlik, J. Cerv, J. Benesš, Analytical, computational and experimental investigation on stress wave propagation, *Applied Mechanics Review* 2 (47) (1994) 77–99.
[6] R. Burridge. Some Mathematical Topics in Seismology, PhD Thesis, New York Univeristy, 1976.
[7] Y.-H. Pao, Elastic waves in solids, *Journal of Applied Mechanics* 50 (1983) 1152–1164.
[8] Y.-H. Pao, R.G. Gajewski, A.N. Ceranoglu, Acoustic emission and transient waves in an elastic plate, *Journal of Acoustical Society of America* 1 (65) (1979) 96–105.
[9] F.R. Breckenridge, C.E. Tschieff, M. Greenspan, Acoustic emission: some applications of Lamb's problem, *Journal of Acoustical Society of America* 3 (57) (1975) 626–631.
[10] J.E. Michaels, T.E. Michaels, W. Sachse, Application of deconvolution to acoustic emission signal analysis, *Materials Evaluation* 39 (1981) 1032–1036.
[11] Z. Shi, J. Jarzynski, L. Jacobs, Study of acoustic emission in plates using finite element method and laser-ultrasonics, *Review of Progress in Quantitative Nondestructive Evaluation* 20 (2001) 1761–1767.
[12] W.H. Prosser, M.A. Hamstad, J. Gary, A. O'Gallagher, Reflections of AE waves in finite plates: finite element modeling and experimental measurements, *Journal of Acoustic Emission* 1–2 (17) (1999) 37–47.
[13] F. Moser, L. Jacobs, J. Qu, Modeling elastic wave propagation in waveguides with the finite element method, *NDT&E International* 32 (1999) 225–234.

[14] M.A. Hamstad, A. O'Gallagher, J. Gary, Modeling of buried monopole and dipole sources of acoustic emission with finite element technique, *Journal of Acoustic Emission* 3/4 (17) (1999) 97–110.
[15] M.A. Hamstad, J. Gary, A. O'Gallagher, Far-field acoustic emission waves by three-dimensional finite element modeling of pencil-lead breaks on a thick plate, *Journal of Acoustic Emission* 2 (14) (1996) 103–114.
[16] J. Gary, M.A. Hamstad, On the far-field structure of waves generated by a pencil lead break on a thin plate, *Journal of Acoustic Emission* 3/4 (12) (1994) 157–170.
[17] Ansys Release 8.1 Documentation, ANSYS, Inc., 2004.
[18] L. Bergmann, *Der ultraschall und seine anwendungen in wissenschaft und technik*, Hirzel Verlag, Stuttgart, 1954.
[19] K. Aki, P.G. Richards, *Quantitative Seismology*, University Science Books, Sausalito, CA, 2002 2nd.
[20] N.N. Hsu, *Dynamic Green's Functions of an Infinite Plate—A Computer Program*, NBS (NIST), 1985.
[21] J. Thomas M. Proctor, An improved piezoelectric acoustic emission transducer, *Journal of Acoustical Society of America* 5 (71) (1982) 1163–1168.
[22] J.R. Webster, Vibro-Acoustic Emission Due to Rubbing and Impact Sources in Vibrating Structures, PhD Thesis, University of Nottingham, 1987.
[23] M.J. Evans. The Use of the Diffuse Field Measurement for Acoustic Emission, PhD Thesis, University of London, 1997.
[24] S.P. Timoshenko, J.N. Goodier, *Theory of Elasticity*, third ed, McGraw-Hill, New York; London, 1970.
[25] F.R. Breckenridge, T. Proctor, N.N. Hsu, S. Fick, D. Eitzen, Transient sources for acoustic emission work, Progress in Acoustic Emission V, Tokyo, 1990, pp. 20–37.